Published in final edited form as:
Sens Actuators B Chem. 2007 April 10; 123(1): 606–613.

Resonance wavelength-dependent signal of absorptive particles in surface plasmon resonance-based detection

Elain Fu[a], **Stephen A. Ramsey**[b], **Jingyi Chen**[c], **Timothy M. Chinowsky**[d], **Benjamin Wiley**[c], **Younan Xia**[c], and **Paul Yager**[a]

a*Department of Bioengineering, University of Washington, Seattle, WA*

b*Institute for Systems Biology, Seattle, WA*

c*Department of Chemistry, University of Washington, Seattle, WA*

d*Department of Electrical Engineering, University of Washington, Seattle, WA*

Abstract

We describe the resonance wavelength-dependent signal of absorptive particles in surface plasmon resonance (SPR)-based detection using both modeling and experimental results. The particles, gold nanocages, have a significant absorption cross-section in the nearinfrared (NIR), resulting in a wavelength-dependent refractive index as measured by SPR. The SPR signal due to the nanocages varies by 4-fold over resonance wavelengths from 650 nm to 950 nm. The greatest SPR signal occurs at the longest resonance wavelengths; its magnitude is due to the inherent increase in sensitivity of SPR on gold with increasing wavelength and the optical absorption properties of the nanocages.

Introduction

Signal amplification using particle tags is a common method of enhancing the surface plasmon resonance (SPR)-based detection of low molecular weight or low concentration analytes. Amplification tags have included secondary/tertiary antibodies[1], latex particles[2, 3], and liposomes[4]. The most effective tags for SPR-based detection are composed of materials that produce large changes in refractive index (RI) per unit volume of material. For this reason, there has been much interest in metal particle tags. Most notably, Lyon *et al.*[5-7]investigated the use of colloidal gold nanoparticles as amplification tags in SPR-based detection. Optical absorptive effects of the particles resulted in dramatic changes in the shape of the SPR curves. Specifically, SPR curves observed in the presence of the gold colloid were broadened and had a significantly increased minimum reflectivity as compared to SPR curves with no gold colloid on the surface. In these and additional studies[8, 9], the amplification potential of colloidal gold particles at a single excitation wavelength was demonstrated.

The effect of the excitation wavelength on the interaction between the surface plasmon polariton field and nanometer-scale metal particles was investigated experimentally in several systems. Holland and Hall[10, 11]observed the greatest shift in the surface plasmon dispersion relation, in their system of silver islands on planar silver, at excitation wavelengths near the absorbance peak of the silver islands. Kume *et al.*[12]observed the largest degree of broadening and the greatest increase in minimum reflectivity of the surface plasmon curves, in their system of silver particles on planar aluminum, at excitation wavelengths matched to the absorbance

peak of the silver particles. More recently, we reported the experimental observation of similar excitation wavelength-dependent effects in a system of gold nanocages on planar gold[13].

The modulation of the surface plasmon reflectivity curve due to absorptive material has also been investigated theoretically by Kurihara *et al.*[14, 15]They presented a model for absorption-based SPR, treating the sample as a collection of Lorentz oscillators and the active metal layer as a Drude free electron gas. Most notably, their model of absorption-based SPR predicts that the direction of the shift of the resonance depends on the relationship between excitation frequency and sample peak absorption frequency. They also showed qualitative agreement between their model and experimental angle interrogation results from an absorption-based SPR sodium ion sensor.

In this report, we describe the resonance wavelength-dependent signal of alloyed gold/silver nanocages on planar gold using both modeling and experimental results. Our model, which incorporates particle absorption as in the work of Kurihara *et al.*[14, 15], shows good agreement with experimental SPR curves. We find that the SPR signal, as quantified by the normalized sum of the absolute value of the difference curve, depends strongly on the resonance wavelength and varies by 4-fold across the wavelength range from 650 to 950 nm. The greatest SPR signal occurs at the longest resonance wavelengths and is due to a combination of the well-established inherent increase in sensitivity of SPR on gold with increasing wavelength[16, 17]and the optical absorption properties of the nanocages.

Experimental

Nanocage synthesis

A typical procedure for the synthesis of the gold nanocages[18, 19]follows. First, silver nanocubes were synthesized. Approximately 5 mL of ethylene glycol (EG, J. T. Baker, NJ) was heated at 149°C for 8 min under a 0.5 SLPM flow of nitrogen to quickly remove water. The solution was then heated under air for 52 min. Next, two 3 mL EG solutions were simultaneously injected into the hot EG at a rate of 45 mL per hour using a syringe pump (KDS-200, Stoelting, IL). One solution contained 94 mM silver nitrate (Sigma-Aldrich, MO), and the other solution contained 0.22 mM NaCl (Fisher Scientific, PA) and 144 mM poly(vinyl pyrrolidone) (PVP, Sigma-Aldrich, MO, M.W. ≈ 55,000). The PVP concentration was calculated in terms of the repeating unit. Magnetic stirring was applied throughout the synthesis. The solution typically turned yellow, orange, and then clear within the first hour after injection. After approximately 20 hours, the solution became orange-red, indicating the presence of 30 nm silver cubes. The reaction was terminated and the nanocubes were washed with acetone and then water before being dispersed in water for the galvanic replacement reaction. A solution of 5 mg poly(vinyl pyrridone) (Sigma-Aldrich, MO, M.W. ≈ 10,000) in 5 mL de-ionized water was heated to boiling and a 75-μL aliquot of a silver nanocube dispersion (8.1 mM silver) was added to the solution. This diluted dispersion of silver nanocubes was then refluxed for 2 min and then 750 μL of 0.2 mM $HAuCl_4$aqueous solution was added at a rate of 0.8 mL/h using a syringe pump. The solution was refluxed for another 10 min until its color became stable. Vigorous magnetic stirring was applied during the entire process. After the solution cooled to room temperature, a white AgCl precipitate formed that was then dissolved by adding a saturated solution of NaCl. The mixture was then centrifuged at 10,000 rpm for 15 min, and the supernatant containing the dissolved AgCl was decanted. The product was rinsed with water and centrifuged twice, and finally re-dispersed in water until use.

Nanocage characterization

The particles were characterized using scanning electron microscopy (SEM) and atomic emission spectroscopy. SEM samples were prepared by putting a drop of product solution on

a small piece of silicon wafer or a carbon-coated copper grid and then vacuum dried. SEM images were taken using a field-emission microscope (FEI, Sirion, OR) operated at acceleration voltages near 15 kV. Approximately 50 particles were analyzed to characterize their size distribution. The metal content of the nanocages was analyzed using an atomic emission spectrophotometer (Thermo Jarrel Ash Corp., MA) equipped with an inductively coupled plasma system. Emission lines at 242.8 nm and 328.0 nm were used to estimate the percentage of gold and silver within the final product. An absorption spectrum of the particles in solution was obtained using a diode array spectrophotometer (Hewlett-Packard, CA).

SPR measurements

The SPR instrument was a custom built Plasmon IV (Institute of Radio Engineering and Electronics [IREE], Czech Republic) with 4 independent channels. Briefly, light from a tungsten halogen lamp (Avantes, The Netherlands) was collimated, polarized, and coupled to the sample film via a BK-7 prism. The reflected light was then collected by a multichannel spectrometer. The SPR reflectivity spectrum was calculated from $R(\lambda) = \frac{r^{TM}(\lambda) - r^{dark}(\lambda)}{r^{TE}(\lambda) - r^{dark}(\lambda)}$, where $r^{TM}(\lambda)$was the spectrum acquired with transverse-magnetically-polarized light, $r^{TE}(\lambda)$ was the spectrum acquired with transverse-electrically-polarized light, and $r^{dark}(\lambda)$was the dark spectrum (acquired with no incident light). To position the resonance minimum at a given wavelength, the angle of incidence was varied by adjustment of the rotation arms on the instrument (decreasing the angle of incidence increases the resonance wavelength).

SPR substrates were prepared by sputtering 2 nm Cr and 55 nm Au (TTS Ltd., Czech Republic) onto BK7 slides (Schott, Germany). The coated substrates were cleaned in a 5:1:1 solution of water, 30% hydrogen peroxide, and ammonium hydroxide for approximately 10 min at 40-70° C and then stored in water until use. The cleaned substrates were passivated with mercaptoethylamine (MEA from Sigma Aldrich, MO) by incubation in a 3 mM MEA in ethanol solution for approximately 3 h, followed by sonication in ethanol for 10 min. The flowcell was composed of the MEA-treated substrate as the base, a midlayer with channels defined in 70 μm mylar/adhesive, and a capping layer of acrylic. All solutions were hand-injected using syringes.

First, water was introduced into a channel and reflectivity spectra were acquired at the three resonance wavelengths of 674 nm, 777 nm, and 927 nm. Next, a nanocage solution of approximately 0.2 nM was introduced into the channel and incubated for approximately 30 min. The nanocage solution was then rinsed from the channel with approximately 10 system volumes of water and reflectivity spectra again acquired at the different resonance wavelengths. A reference channel containing water was monitored throughout the experiment and indicated that the effects of temperature and instrument drift were minimal. The surface coverage of nanocages for the sample was estimated by counting particles in 2 μm × 2 μm regions sampled over an area of 10 μm × 15 μm using SEM at acceleration voltages near 5 kV.

Modeling

The experimental data was modeled in a two-stage process. In each stage, optimization on multiple parameters was performed at the three experimental resonance wavelengths of 674 nm, 777 nm, and 927 nm to obtain the best fit to the experimental data. The SPR model was custom coded in MATLAB. Optimization was performed using a constrained branch and fit algorithm by Huyer and Neumaier[20]. The goodness-of-fit parameter was defined as a weighted sum of the squares of the difference between the experimental and simulated reflectivity curves. The weighting factor, the inverse square of the experimental reflectivity curve, was chosen to emphasize the region about the minimum of the SPR curve.

In the first stage, the MEA-only sample was modeled as a five-layer system composed of prism, chromium layer, gold layer, MEA layer, and water. Optimization to obtain the best fit to the experimental SPR curves for the MEA-only sample was performed simultaneously at the three resonance wavelengths. The refractive indices of the MEA layer and water, assumed to be constant with respect to wavelength, were modeled as 1.5 and 1.333 respectively. The dispersion relations of the prism, chromium, and gold layers were modeled using polynomial fits to values of the wavelength-dependent refractive indices reported in the literature. In the case of gold, the literature values corresponded to electropolished gold [110][21]. It is expected that the RI of the sputtered gold layer used in the experiment will vary significantly from the RI of the electropolished gold. Thus, the imaginary part of the gold layer RI used in the model was subsequently allowed to vary to within 40% of the above literature values. The gold thickness was allowed to vary within 5% of the experimental target thickness of 55 nm. Additionally, the angle of incidence for each of the resonance wavelengths was allowed to vary in a range of ± 1°. An experimental angle spread of 0.3° was assumed (estimate from IREE) in all cases. Table 1lists the optimized values of the relevant parameters.

In the second stage, the MEA-plus-nanocage sample was modeled as a six-layer system composed of prism, chromium layer, gold layer, MEA layer, nanocage layer, and water. The set of best fit parameters obtained for the five-layer system in the first stage was fixed, and the MEA-plus-nanocage sample was modeled at the three resonance wavelengths. The nanocage layer was modeled as a collection of Lorentz oscillators after Kurihara *et al*.[14, 15]The expression used for the permittivity of the nanocage layer is

$\varepsilon_{ns} = \varepsilon_{ns}^{background} + f(N)\frac{\omega_0^2}{\omega_0^2 - \omega^2 - i\omega\gamma}$, where ω is the angular frequency of incident light, $\omega_0 = \frac{2\pi c}{\lambda_{\max}}$ is the oscillator angular frequency, *f(N)* is the oscillator strength (proportional to the number density of particles, *N*), and $\gamma = \frac{2\pi c\lambda_{FWHM}}{\lambda_{\max}^2}$ is the oscillator damping angular frequency. Here$\lambda_{\max}$is the peak absorption wavelength of the nanocages,$\lambda_{FWHM}$is the full width at half maximum (FWHM) of the absorption peak of the nanocages, and *c*is the speed of light in vacuum. The parameter $\varepsilon_{ns}^{background}$is the frequency-independent background permittivity. The parameters $f(N)$,λ_{FWHM},$\lambda_{\max}$, and $\varepsilon_{ns}^{background}$were simultaneously varied under constrained optimization. The optimized values of these parameters are listed in Table 1.

Results and Discussion

An SEM image of the nanocages used for size characterization is shown in Figure 1. The average edge length was measured to be 40 ± 5 nm. The gold:silver ratio of the nanocages was approximately 4:1, producing an absorption peak in the near infrared (NIR) with a peak wavelength of 795 nm and a full width at half maximum (FWHM) of 150 nm for nanocages in solution. However, the absorption peak of the nanocages will be influenced by the proximity of the nanocages to the planar gold. Reports in the literature on other metal nanoparticles show that the absorption peaks are significantly red-shifted[22, 23], consistent with the modeling results below. The surface coverage of the nanocages was estimated from SEM to be approximately 1×10^9particles/cm^2(approximately 10% of the area density of a close-packed monolayer). SPR measurements at three different surface coverages of similarly sized nanocages indicated that the maximum change in reflectivity is approximately linear with surface coverage below 3×10^9particles/cm^2(as measured by an alternate SPR-based instrument, data not shown).

The SPR curves for the MEA-only sample and MEA-plus-nanocages sample at each of the three incident angles are shown in Figure 2. The nanocages produce three main effects on the SPR curve. The SPR curve is broadened with respect to the MEA-only curve, its minimum reflectivity increases, and its minimum is shifted to lower wavelengths (corresponding to greater incident angle, for angle interrogation measurements) with respect to the MEA-only sample. These results are consistent with the observations of Lyon *et al.*using gold colloid[5-7]. Most notably, the *degree of modulation*of the SPR curve depends on the resonance wavelength. At 674 nm, the effects, though measurable, are small in magnitude. The modulation effects are increased at 777 nm and greatest at 927 nm.

The difference between the MEA-plus-nanocages sample and the MEA-only sample is shown in Figure 3, for three resonance wavelengths. One measure of the signal change due to absorptive particles used in previous reports[5, 24]is the maximum change in reflectivity; with this measure, the signal change due to nanocages is approximately 9% at 674 nm, 23% at 777 nm, and 37% at 927 nm. Alternative measures, which more completely describe the quantifiable difference in signal have been discussed in detail[25]. In this study, we use the normalized sum of the absolute value of the difference curve. Specifically, the sum of the absolute value of the difference curve is multiplied by the range of wavelengths interrogated and divided by the total number of data points in the range of wavelengths interrogated. Since this measure depends on the difference curve across the entire investigated wavelength range, it should be more sensitive to the nanocage-induced modulation of the SPR curve, as compared to the maximum change in reflectivity. The normalized sum of the absolute value of the difference curve is 15.3 for the resonance at 674 nm, 40.1 for the resonance at 777 nm, and 65.6 for the resonance at 927 nm.

The model and experimental SPR curves for the MEA-only sample at the three resonance wavelengths are plotted together in Figure 4A-Cand show good agreement. The imaginary part of the gold RI used in the model as well as the literature values for electropolished gold [110] are shown in Figure 4D. The model and experimental SPR curves for the MEA-plus-nanocages sample are shown in Figure 5A-C; here again, good agreement is observed between the model and experimental data. The optimized model results indicate a nanocage absorption peak centered at 920 nm with a FWHM of 214 nm. The imaginary part of the nanocage RI used to obtain the model results is shown in Figure 5D. The parameters used in the model are listed in Table 1.

The SPR signal of the nanocages, as measured by the normalized sum of the absolute value of the difference curve, as a function of resonance wavelength is shown in Figure 6A. The model and experimental results indicate that the magnitude of the signal varies by 4-fold over the wavelength range investigated. This increase is due in part to the NIR absorption peak of the nanocages. However, a greater sensitivity is also achieved at longer wavelengths for non-absorptive samples on planar gold[16, 17]. Also shown for comparison is the model result of the signal change for the replacement (above the MEA layer) of a non-absorbing bulk solution with $\Delta RI=0.001$ RIU. As expected, the non-absorbing bulk solution exhibits signal enhancement at the longer wavelengths, though less than the absorptive nanocages.

Model results of the effect of nanocage absorption peak wavelength on the SPR signal are shown in Figure 6B. All other parameters of the system are unchanged. Note that it would be impossible to synthesize nanocages that were similar in all respects except for the wavelength of the absorption peak. Nonetheless, these model results are useful for exploring the relative effects of 1) matching the wavelength of the particle absorption peak to the resonance wavelength and 2) using longer resonance wavelengths to enhance sensitivity. The results suggest that for a given resonance wavelength, the particle absorption peak wavelength does have a significant impact on the SPR signal. However, the dominant effect is the inherent

greater sensitivity at longer wavelengths. In the context of the model, the greatest signal will be achieved at long resonance wavelengths for a particle with a long-wavelength absorption peak.

Conclusion

We have demonstrated the resonance wavelength-dependent SPR signal of nanocage particles using both modeling and experimental results. A simple model of SPR reflectivity incorporating the absorptive effects of the particles was demonstrated to be in good agreement with the experimental results. The SPR signal of the particles was shown to vary by a factor of 4 across the range of resonance wavelengths investigated and was greatest at the longest wavelengths. The magnitude of the SPR signal in the NIR was due to a combination of two effects: (1) the inherent increase of the SPR signal on gold at longer wavelengths and (2) the absorption peak of the particles in the NIR. The absorptive SPR model could serve as a useful tool to probe the relationship between particle absorption properties and the SPR signal as a function of resonance wavelength for a number of recently reported particles systems with tunable optical absorption properties.

Acknowledgements

The authors (EF, TC, and PY) gratefully acknowledge financial support from NIDCR grant number 1U01 DE014971. The authors gratefully acknowledge the Center for Nanotechnology at the University of Washington for the use of their facilities. EF thanks Marek Piliarik for helpful discussions.

References

1. Naimushin A, Soelberg S, Bartholomew D, Elkind J, Furlong C. A portable surface plasmon resonance sensor system with temperature regulation. Sensors and Actuators B 2003;96:253–260.
2. Besselink GAJ, Kooyman RPH, van Os P, Engbers GHM, Schasfoort RBM. Signal amplification on planar and gel-type sensor surfaces in surface plasmon resonance-based detection of prostate-specific antigen. Analytical Biochemistry 2004;333:165–173. [PubMed: 15351293]
3. Devries EFA, Schasfoort RBM, Vanderplas J, Greve J. Nucleic-Acid Detection with Surface-Plasmon Resonance Using Cationic Latex. Biosensors & Bioelectronics 1994;9:509–514.
4. Wink T, van Zuilen S, Bult A, van Bennekom W. Liposome-mediated enhancement of the sensitivity in immunoassays of proteins and peptides in surface plasmon resonance spectroscopy. Analytical Chemistry 1998;70:827–832. [PubMed: 9511463]
5. Lyon L, Musick M, Natan M. Colloidal Au-enhanced surface plasmon resonance immunosensing. Analytical Chemistry 1998;70:5177–5183. [PubMed: 9868916]
6. Lyon LA, et al. Surface plasmon resonance of colloidal Au-modified gold films. Sensors and Actuators B-Chemical 1999;54:118–124.
7. Lyon LA, Pena DJ, Natan MJ. Surface plasmon resonance of Au colloidmodified Au films: Particle size dependence. Journal of Physical Chemistry B 1999;103:5826–5831.
8. Mitchell JS, Wu YQ, Cook CJ, Main L. Sensitivity enhancement of surface plasmon resonance biosensing of small molecules. Analytical Biochemistry 2005;343:125–135. [PubMed: 15950915]
9. Pieper-Furst U, Stocklein WFM, Warsinke A. Gold nanoparticle-enhanced surface plasmon resonance measurement with a highly sensitive quantification for human tissue inhibitor of metalloproteinases-2. Analytica Chimica Acta 2005;550:69–76.
10. Holland WR, Hall DG. Optical-Properties of Metal Particles near Conducting Surfaces. Journal of the Optical Society of America 1982;72:1747–1747.
11. Holland WR, Hall DG. Surface-Plasmon Dispersion-Relation - Shifts Induced by the Interaction with Localized Plasma Resonances. Physical Review B 1983;27:7765–7768.
12. Kume T, Nakagawa N, Hayashi S, Yamamoto K. Interaction between Localized and Propagating Surface-Plasmons - Ag Fine Particles on Al Surface. Solid State Communications 1995;93:171–175.
13. Fu, E., et al. Microtas 2005 . Jensen, K.; Han, J.; Harrison, D.; Voldman, J., editors. Boston : 2005. p. 1510-1512.

14. Kurihara K, Nakamura K, Hirayama E, Suzuki K. An absorption-based surface plasmon resonance sensor applied to sodium ion sensing based on an ion-selective optode membrane. Analytical Chemistry 2002;74:6323–6333. [PubMed: 12510755]
15. Kurihara K, Suzuki K. Theoretical understanding of an absorption-based surface plasmon resonance sensor based on Kretchmann's theory. Analytical Chemistry 2002;74:696–701. [PubMed: 11838698]
16. de Bruijn H, Kooyman R, Greve J. Choice of metal and wavelength for surface-plasmon resonance sensors: some considerations. Applied Optics 1992;31:440–442.
17. Homola J. On the sensitivty of surface plasmon resonance sensors with spectral interrogation. Sensors and Actuators B 1997;41:207–211.
18. Chen J, et al. Gold nanocages: Engineering the structure for biomedical applications. Advanced Materials 2005;17:2255–2261.
19. Sun Y, Xia Y. Mechanistic study on the replacement reaction between silver nanostructures and chloroauric acid in aqueous medium. Journal of the American Chemical Society 2004;126:3892–3901. [PubMed: 15038743]
20. Huyer W, Neumaier A. SNOBFIT-Stable noisy optimization by branch and fit. 2006Submitted to ACM Transactions on Mathematical Software
21. Weast, R.; Lide, D.; Astle, M.; Beyer, W., editors. CRC Handbook of Chemistry and Physics. CRC Press Inc; Boca Raton: 1989.
22. Okamoto T, Yamguchi I. Optical absorption study of the surface plasmon resonance in gold nanoparticles immobilized onto a gold substrate by self-assembly technique. The Journal of Physical Chemistry B 2003;107:10321–10324.
23. Pinchuk A, Hilger A, von Plessen G, Kreibig U. Substrate effect on the optical response of silver nanoparticles. Nanotechnology 2004;15:1890–1896.
24. Nelson B, Frutos A, Brockman J, Corn R. Near-infrared surface plasmon resonance measurements of ultrathin-films. 1. angle shift and SPR imaging experiments. Anal Chem 1999;71:3928–3934.
25. Chinowsky T, Yee S. Quantifying the information content of surface plasmon resonance reflection spectra. Sensors and Actuators B 1998;51:321–330.
26. Jung, L. Chemistry . University of Washington; Seattle: 1999.
27. Ulman A. Formation and structure of self-assembled monolayers. Chemical Reviews 1996;96:1533–1554. [PubMed: 11848802]

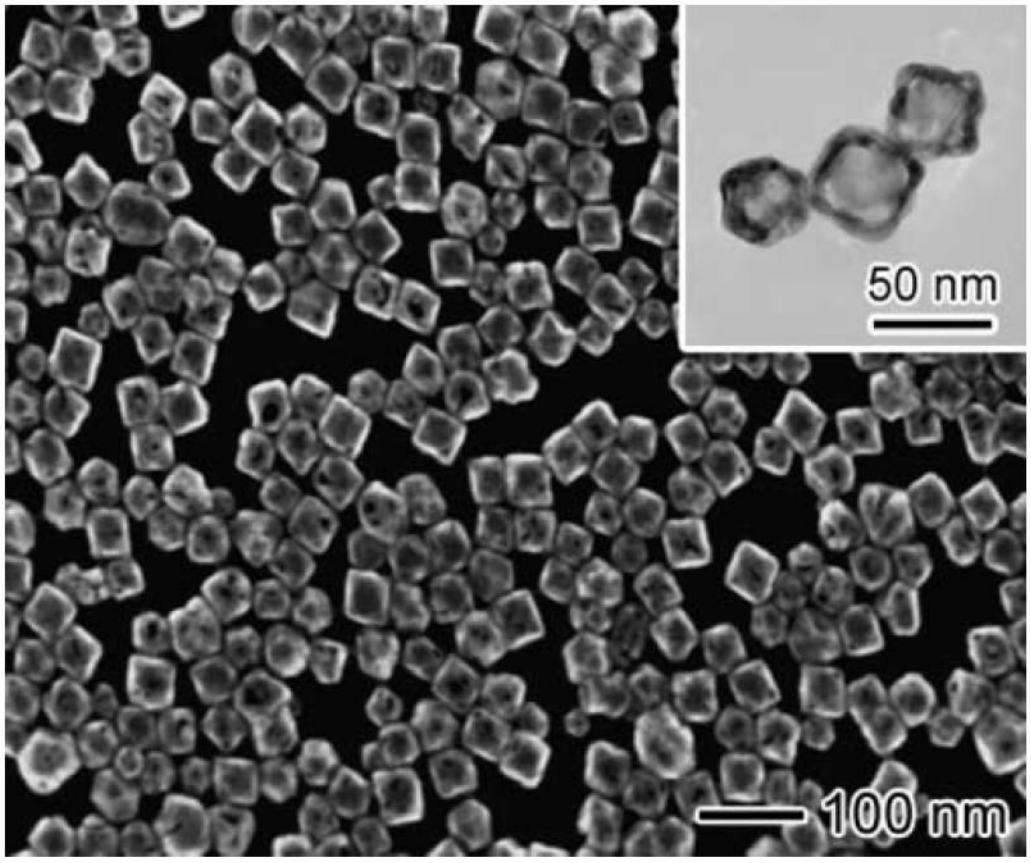

Figure 1.
SEM image of the nanocages. The inset image was acquired with a transmission electron microscope. The nanocages were composed of gold and silver in a ratio of 4:1 and were approximately 40 nm ± 5 nm in edge length.

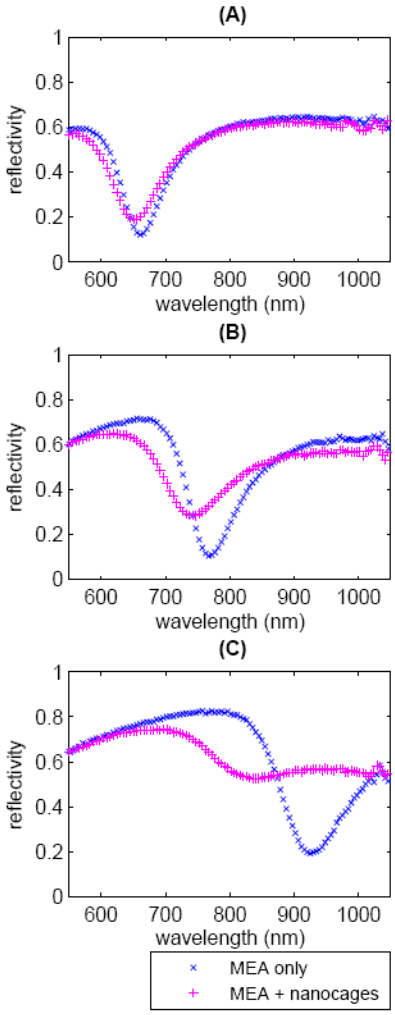

Figure 2.
The SPR curves of the MEA-only sample and the MEA-plus-nanocages sample for the MEA resonance wavelength of (A) 674 nm, (B) 777 nm, and (C) 927 nm. The effects of the nanocages are to broaden, increase the minimum reflectivity of, and shift the resonance wavelength of the SPR curves.

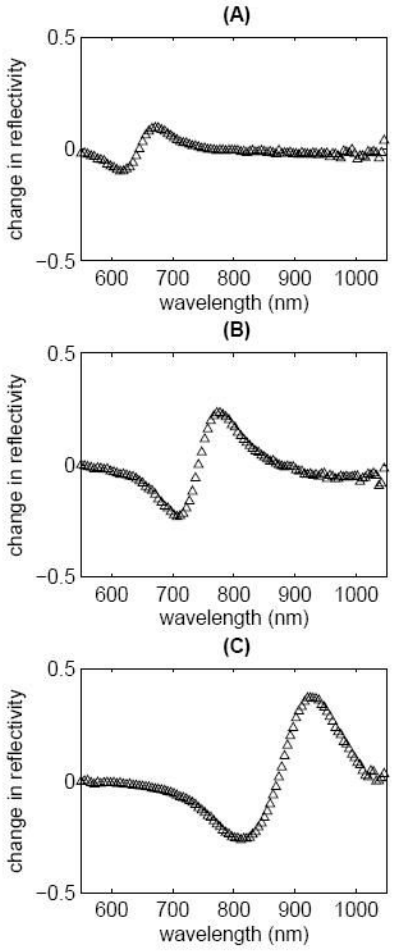

Figure 3.

The difference curve of the MEA-plus-nanocages sample and the MEA-only sample for the MEA resonance wavelength of (A) 674 nm, (B) 777 nm, and (C) 927 nm. The normalized sum of the absolute value of the difference curve can be used to quantify the signal change due to the particles. The normalized sum is 15.3, 40.1, and 65.6 for case (A), (B), and (C), respectively.

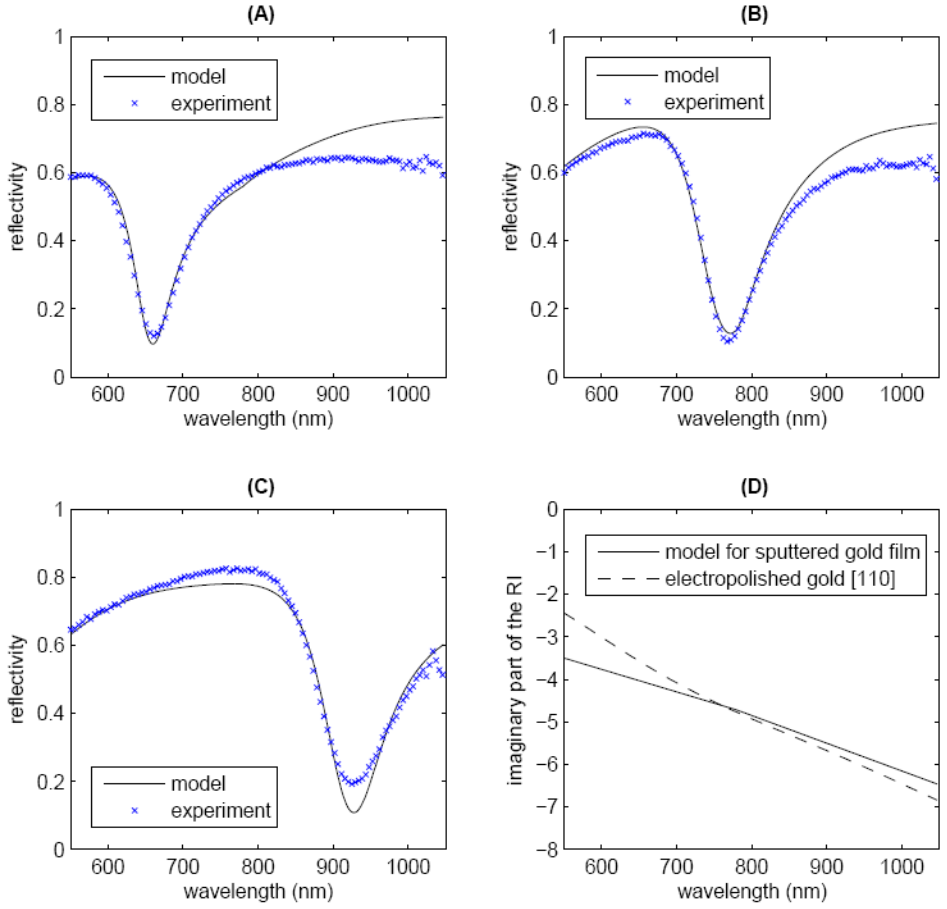

Figure 4.

Comparison of model and experimental SPR curves for the experimental MEA resonance wavelength of (A) 674 nm, (B) 777 nm, and (C) 927 nm show good agreement. (D) The imaginary part of the RI of gold between 550 and 1050 nm. For comparison, the literature values for electropolished gold [110][21]are also shown. The other model parameters are listed in Table 1.

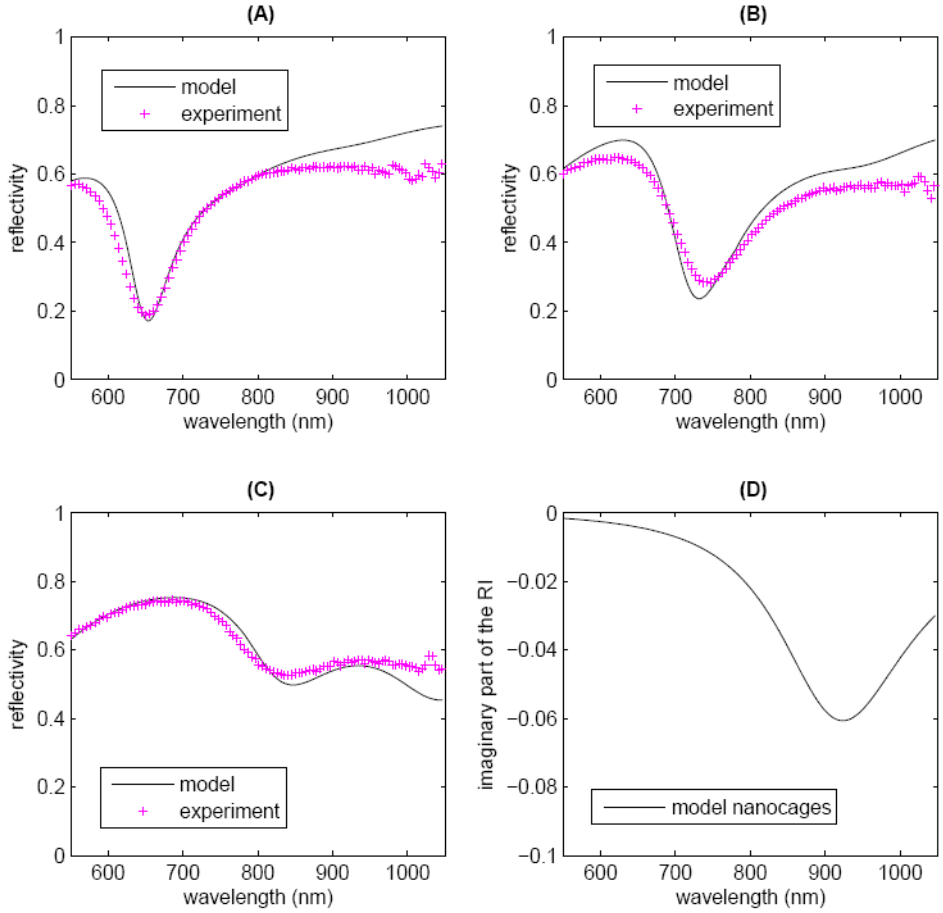

Figure 5.

Comparison of model and experimental SPR curves for MEA plus nanocages for the experimental MEA resonance wavelength of (A) 674 nm, (B) 777 nm, and (C) 927 nm show good agreement. (D) The imaginary part of the RI of the nanocages between 550 and 1050 nm, used in the model. The other model parameters are listed in Table 1.

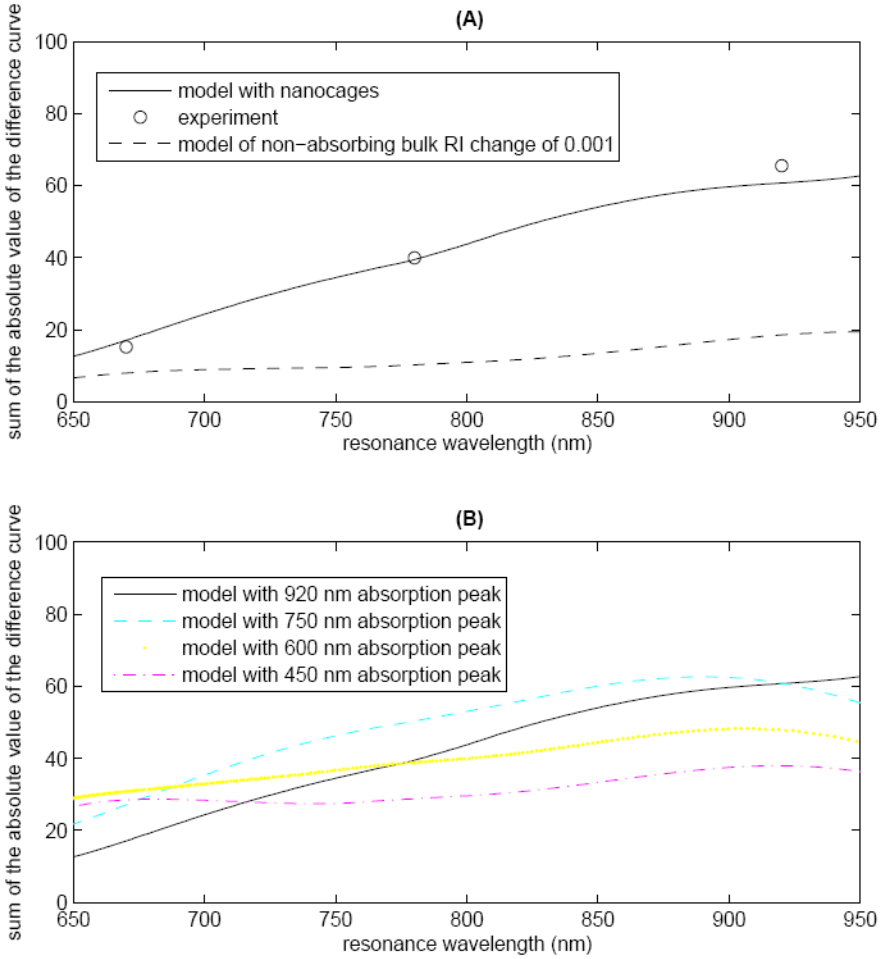

Figure 6.

The SPR signal, the normalized sum of the absolute value of the difference curve of the MEA-only and the MEA-plus-nanocages samples, as a function of resonance wavelength. (A) Model results (solid line) are plotted for resonance wavelengths from 650 nm to 950 nm with the experimental data points (o) overlaid. For comparison, the model result of the signal change due to the replacement of a non-absorbing bulk solution with ΔRI=0.001 RIU above the MEA layer is shown (-). (B) Model results of the effect of shifting the wavelength of the particle absorption peak. All other parameters are unchanged. The results suggest that for a given resonance wavelength, the particle absorption peak wavelength does have a significant impact on the SPR signal. However, for a particle with a given absorption peak wavelength, the dominant effect is the greater sensitivity at longer wavelengths.

Table 1

The table lists the model input parameters

Parameter	Model
BK7 prism RI	Schott dispersion formula
BK7 thickness	Semi-infinite
Chromium RI	8^{th}order polynomial fit to values from[21]
Chromium layer thickness	2.5 nm (2 nm target for sputtered film by TTS)
Gold RI	See Figure 3dfor imaginary part 8^{th}order polynomial fit to values from [21]for real part
Gold layer thickness	58 nm (55 nm target for sputtered film by TTS)
MEA RI	1.5[21, 26]
MEA layer thickness	0.5[27]
Nanocage absorption peak	920 nm
Nanocage absorption FWHM	214 nm
Nanocage layer thickness	40 nm (40+/-5 nm as measured from SEM images)
Nanocage oscillator strength	4×10^5
Nanocage layer background ε	1.803 (1.343)
Water RI	1.333
Water layer thickness	Semi-infinite
Angle spread	0.3° (estimate from IREE)